Journal of Magnetism and Magnetic Materials 394 (2015) 274–279

Contents lists available at ScienceDirect

Journal of Magnetism and Magnetic Materials

journal homepage: www.elsevier.com/locate/jmmm

Correlation between coercive field and radiation attenuation in Ni and Mg ferrite doped with Mn and Co

José Eves M. Silva [a], Ricardo S. Nasar [a], Marinalva C. Nasar [a], Caio L. Firme [a], José H. Araújo [b]

[a] Chemistry Institute, UFRN, Cep. 59078-970, Natal, do Norte, Brazil
[b] Department of Theoretical and Experimental Physics, UFRN, Cep. 59078-970, Natal, Grande do Norte, Brazil

ARTICLE INFO

Article history:
Received 16 March 2015
Received in revised form
21 May 2015
Accepted 4 June 2015
Available online 14 June 2015

Keywords:
Spinel ferrite
Citrate precursors
Magnetic material
Radar absorbing material
Ferrimagnetic materials
Magnetic coercivity and reflectivity

ABSTRACT

It was investigated $NiMg_{0.1}M_xFe_2O_4$ ferrite where M stands for Mn, Co or simultaneously Mn and Co dopants. The concentration of M is 0.1 and it was divided by two in the sample with addition of Mn and Co. It was used the method of citrate precursors with 1100 °C calcination. The materials were characterized by X-ray diffractometer (XRD), scanning electron microscopy (SEM), vibrating sample magnetometer (VSM) and reflectivity measures by waveguide method. The X-ray diffraction measures, with Rietveld refinement, present average crystallite sizes between 0.576 and 0.626 μm. The SEM analysis shows clustered particles smaller than 1 μm at 1100 °C, in agreement with Rietveld refinement. The compositions with Mn reach magnetization between 42.09 and 53.20 Am^2/kg, which does not generate high microwave absorption. The 0.1 Co addition reached greater coercivity (2.96×10^{-2} T), with up to 84% reflectivity at 10.17 GHz frequency. The Co material has high magnetocrystalline anisotropy, which is associated with the increase of coercive field, H_c. The higher coercivity optimizes the reflectivity results.

1. Introduction

There has been a great challenge to rationalize the processing technology of radar absorbing materials, RAM, [1,2,3,4]. Successful usages of these materials are: in aeronautics with the aim of reducing the detection of a target by a radar; in telecommunications, where the magnetic nuclei are used to eliminate the microwave band radiation in large scale equipment; in electronics, where the cabling systems that reduce or eliminate spurious radiation caused by electronic gadgets; in army, for the intelligent monitoring of camouflage; in medicine, for the radiation shielding of medical equipment. These materials are manufactured by compatibility and electromagnetic interference industry [2,3]. In order to boost technological headway it is needed the combination of components with proper electric and magnetic properties [2,5,6,7]. However, as to oxide ceramics such as ferrites, the composition, the synthesis parameters and the intrinsic characteristics (magnetic saturation, permeability and magnetic permittivity) are associated with their structural properties [6,8,9,10]. This has become decisive for obtaining high performance technological materials [11–17] .

In ferrites with Ni $Mg_{0,1} \cdot M_xFe_2O_4$ general formula, the partial substitution of Fe^{+3}, Ni^{+2} and Mg^{+2} ions at positions A or B by Mn^{+2} and Co^{+2} ions yields modifications of the magnetic properties and their microwave absorption. Aiming to investigate these changes, $NiMgM_xFe_2O_4$ phases were synthesized, where M represents Mn, Co or simultaneously Mn and Co dopant and $x=0.1$, and their powders were physical-chemically characterized. In this work, the studied compositions were obtained by one of most effective methods for synthesizing ferrites which is the process of citrate precursors [7,8,9,11]. In this work, we highlight the influence of thermal treatment, the chemical composition, and the hysteresis characteristics (Hc) in the absorption of electromagnetic radiation of these materials.

2. Experimental

The a: $NiMgMnFe_2O_4$, b: $NiMgCoFe_2O_4$ and c: $NiMgMnCoFe_2O_4$ compositions were prepared according to the method of citrate precursors. The reactants were the citric acid ($C_6H_8O_7 \cdot H_2O$; Nuclear) and nitrates: $Ni(NO_3)_2 \cdot 6H_2O$ Aldrich), $Mg(NO_3)_2 \cdot 6H_2O$ Aldrich), $Mn(NO_3)_2 \cdot 6H_2O$ Aldrich), $Co(NO_3)_2 \cdot 6H_2O$ (98% Aldrich) and $Fe(NO_3)_2 \cdot 9H_2O$ (98% – Aldrich). The citric acid is able to coordinate to metallic ions, which enhances the mixture homogeneity during the formation of citrates.

The stoichiometric solution was heated at 80 °C for 2 h under magnetic stirring. During the heating, it was formed a homogeneous system among the metallic citrates. The homogenized solutions were calcined in a furnace, at 10 heating rate for

E-mail addresses: evesquimica@yahoo.com.br (J.E.M. Silva), nasar@terra.com.br (R.S. Nasar), mari.nat@terra.com.br (M.C. Nasar), humberto@dfte.ufrn.br (J.H. Araújo).

http://dx.doi.org/10.1016/j.jmmm.2015.06.014
0304-8853/

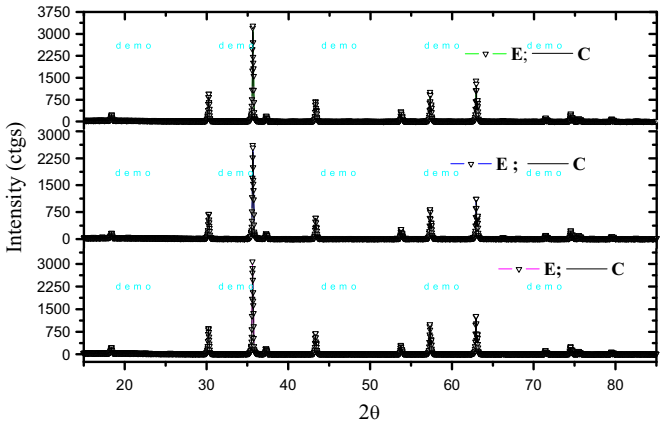

Fig. 1. X ray diffraction pattern and Rietveld analysis of $NiMg_{0.1}M_xFe_2O_4$ composition, for *x*: (a) 0.1 of Mn; (b) 0.1 of Co and (c) 0.05 Mn and 0.05 Co. Triangular trace represents experimental (E) values and straight line represents calculated (C) values from Rietveld.

Table 1
Quantity of dopants and Rietveld refinement estimate of Sig, R_W(%), *a*(Å) e (nm) for a, b and c compositions. Materials were calcined at 1100 °C.

Composition	*x*/*y*	Sig	$R_{w(\%)}$	*a*(Å)	(nm)
a	0.10/0	1.413	21.228	8.346	625.300
b	0/0.10	1.370	22.040	8.343	575.600
c	0.05/0.05	1.343	20.376	8.344	626.200

X/*Y*: ratio of quantity of Mn and quantity of Co. *a*: cell parameter obtained by Rietveld technique. *b*: crystallite size obtained by Rietveld technique.

calcination. The calcination was at 350 °C for 3.5 h and afterwards the powders were decoupled and seived in a 325 ABNT/ASTM mesh sieve. The compositions were calcined at 1100 °C limit temperature for h in ambient atmosphere.

For the X-ray diffraction analysis it was used a Shimadzu XRD 6000 diffractometer, 30 kV tube voltage, 30 mA tube current, CuKα radiation (λ = 1.5418 Å), 2θ step angle = 2 °/min (15° and 85°). The X-ray diffraction results were further analyzed by Rietveld refinement with MAUD software, v. 2.044 [11]. The scanning electron microscopy (SEM) data were obtained from Philips XL-30-ESEM equipment. For vibrating sample magnetometry (VSM) it was used LMMM equipment to measure MxT at −196 to 377 °C temperature range. The magnetic field ranged from −15 to 15 Oe. The reflectivity measures derived from the waveguide method using an equipment developed by IAE/DCTA in the range of 8.2–12.4 GHz [3,4,18] where the RAM materials were prepared by the mixture with epoxy resin (Araldite Profissional – CIBA) and further added into a mold [18]. The molds were plunged in a demolding solution and placed over a 100% reflective metallic plate. The mixture of raw material was done from resin weighing and addition of ferrite powder at 50% mass over total weight.

The theoretical magnetization (M_T) was calculated according to components of spin angular momentum depicted in Eq. 1. The values of M_T follow the antiferromagnetic model of Néel for T = 0 K [12,13,16].

$$M_T = 5(Fe_{oct.} - Fe_{tet.}) + 5(Mn_{tet.} - Mn_{oct.}) + 3(Co_{oct.} - Co_{tet.}) + 2(Ni_{oct.} - Ni_{tet.}) \quad (1)$$

where *x* stands for *x* ions in tetrahedral sites; and $x_{(oct.)}$ stands for x ions in octahedral sites.

The factors 5, 3 and 2 in Eq. 1 represent the magnetization

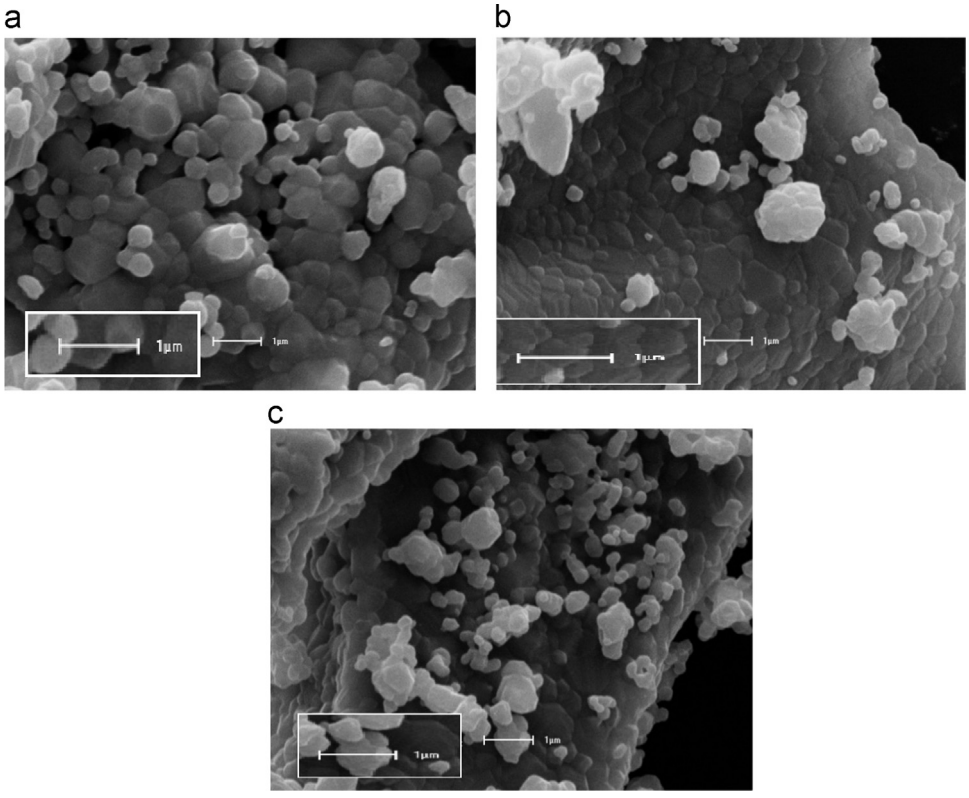

Fig. 2. Scanning electron microscopy of $Ni_{0.8}Mg_{0.1}M_xFe_2O_4$ compositions, for *x*, a: 0.1 of Mn, b: 0.1 of Co and c: 0.05 Mn and 0.05 Co, calcined at 1100 °C. Magnification of 1000 × .

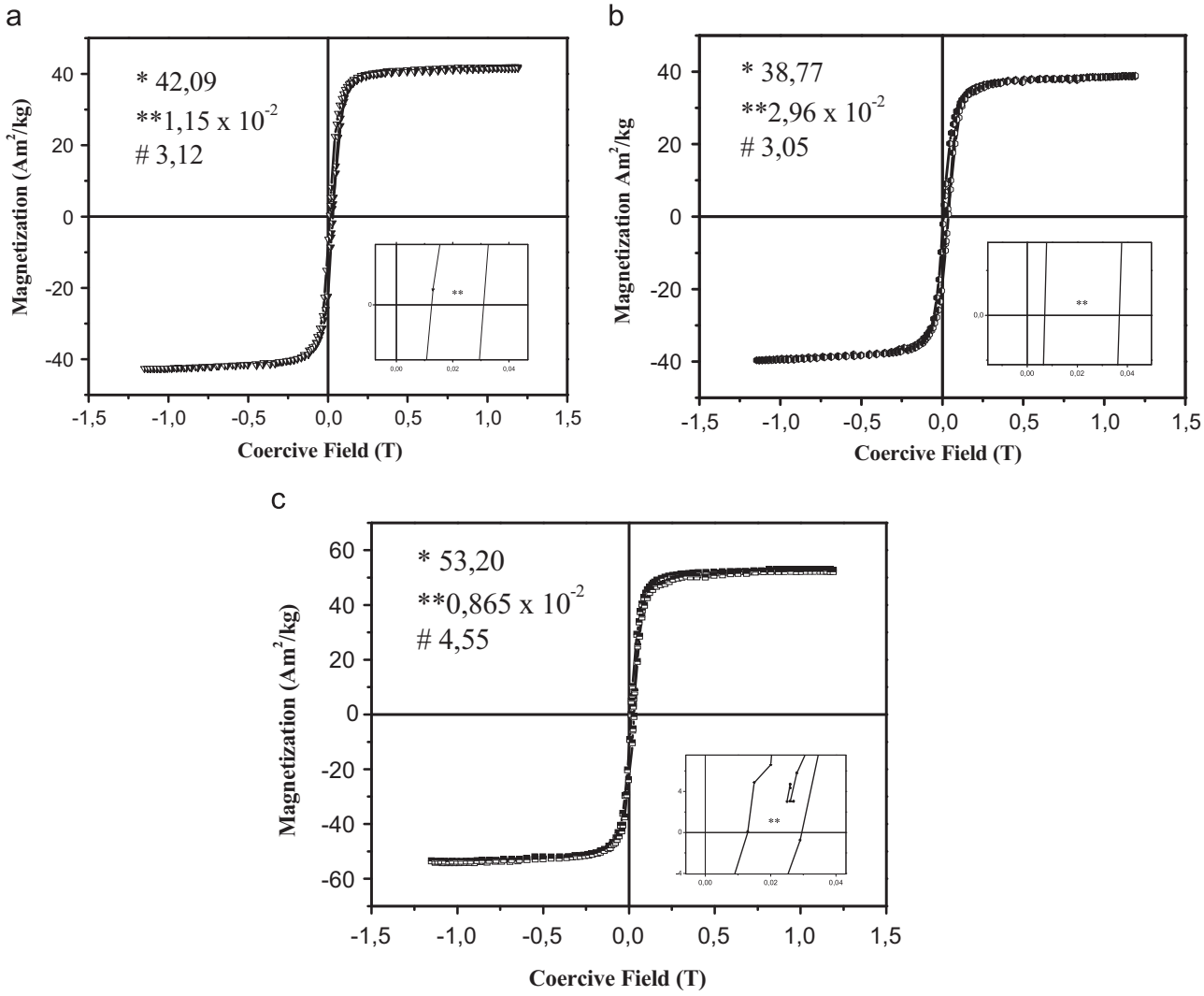

Fig. 3. Magnetic hystheresis of $NiMg_{0.1}M_xFe_2O_4$ composition, for *x*, a: 0.1 of Mn; b: 0.1 of Co and c: 0.05 Mn and 0.05 Co. Powder calcined at 1100 °C/3 h in air ambient. Experimental magnetization saturation (*), Coercive field (**) and theoretical magnetization (#).

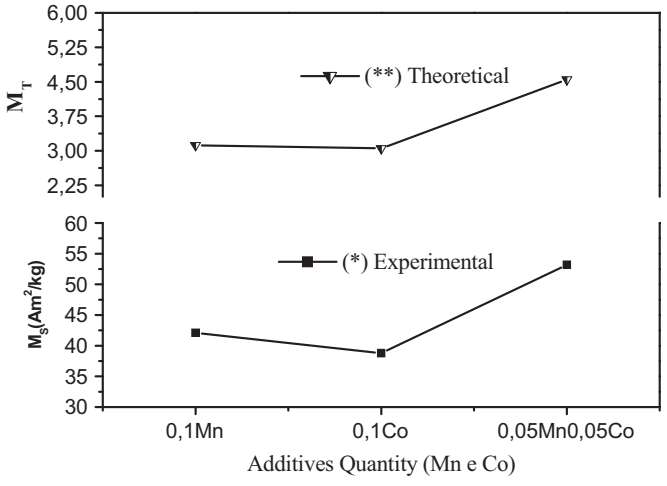

Fig. 4. Experimental magnetization saturation versus dopants quantity (*) and theoretical magnetization versus dopants quantity (**) of $NiMg_{0.1}M_xFe_2O_4$ composition, for x, a: 0.1 of Mn; b: 0.1 of Co and c: 0.05 Mn and 0.05 Co.

according to the spin angular momentum of the corresponding cations.

The Eq. 2 was used to calculate the experimental magnetization ($M_{exp.}$) in Bohr magneton unit. The calculation was done from saturation magnetization (M_s) indicated in the hysteresis cycle of VSM analysis. The values of experimental magnetization were compared with those from theoretical magnetization.

$$M_{exp.} = \frac{MM \times M_s}{N \times B} \quad (2)$$

Where MM is the molar mass, M_s is saturation magnetization, N is Avogadro number and B is the conversion factor to express the magnetic momentum by unit cell, whose value is 9.27×10^{-21} erg/Gauss.

3. Results and discussion

The X-ray diffraction and Rietveld analysis depicted in Figure 1 indicate agreement between experimental and calculated standard. The intensities of 2θ planes from 30, 36, 43.5, 57.5, and 63.5° are more sensitive to Ni^{+2}, Mg^{+2}, Mn^{+2}, Co^{+2}, and Fe^{+2} cations forming tetrahedral and octahedral sites with oxygen atoms [7,8,11]. Calcination temperature and dopants (Mn and Co) effects favor a 100% ferrite phase synthesis with space group Fd-3m:1. The ionic radii of metallic cations occupy tetrahedral and octahedral positions of the structures. This represents a determining

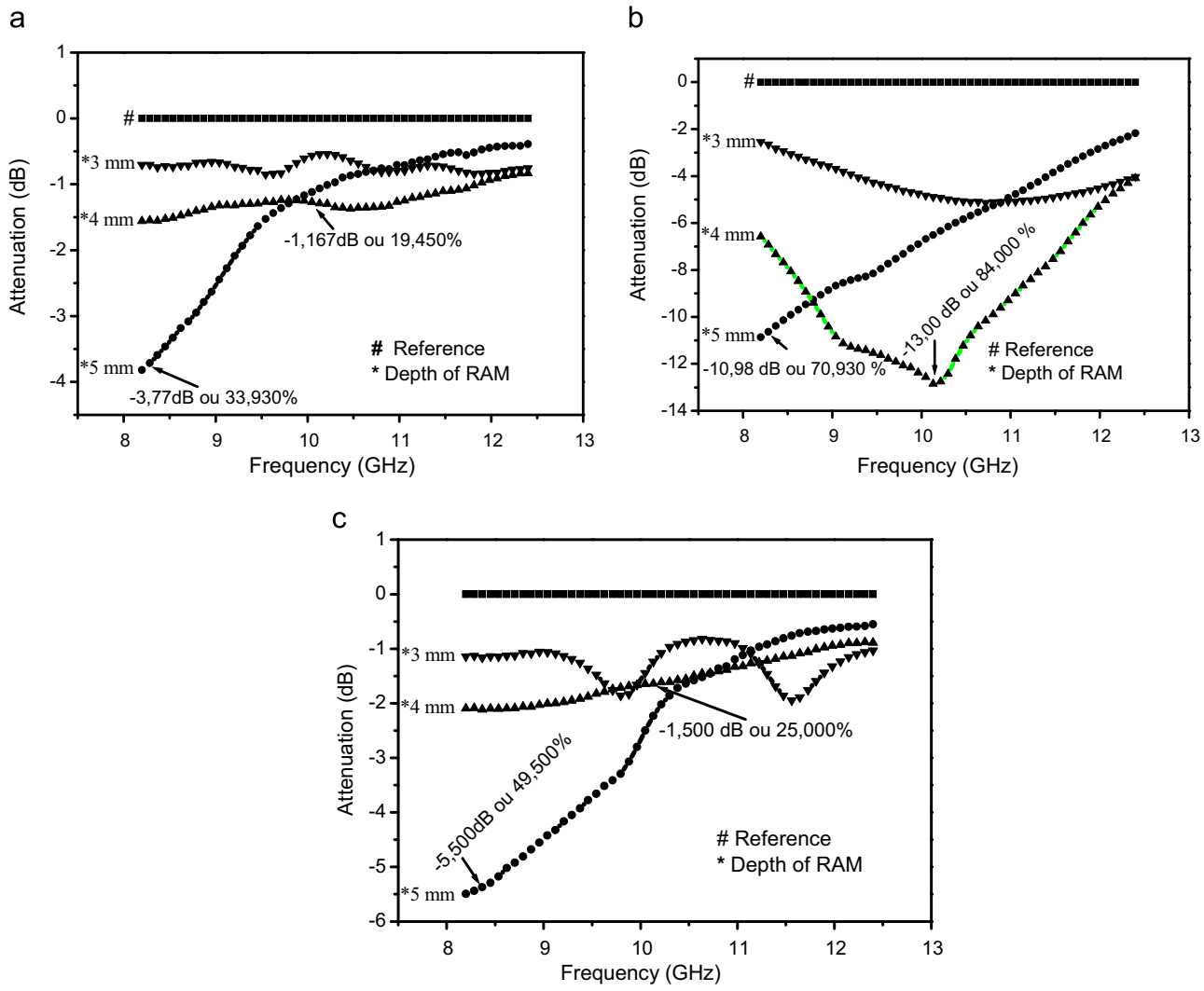

Fig. 5. Reflectivity versus frequency (8.2–12.4 GHz) of $NiMg_{0.1}M_xFe_2O_4$ composition, for *x*, a: 0.1 of Mn; b: 0.1 of Co and c: 0.05 Mn and 0.05 Co, at 1100 °C/3 h.

Table 2
Quantity of dopant, coercive field and percentage of maximum attenuation of the phases at °C.

Composition	Quantity of Mn/Quantity of Co	*H*(T)	(*E*) $Attenuation_{Frequency}$
a	0.1Mn/0.0Co	1.15×10^{-2}	(4) 19. $450_{10.17}$%
b	0.0Mn/0.1Co	2.96×10^{-2}	(4) 84.$000_{10.17}$%
c	0.05Mn/0.05Co	8.65×10^{-3}	(4) 25.$000_{10.17}$%

(*E*): Depth in mm. *H*(T): Coercive field in T.

factor in values of *a*(Å) [11]. When we compare the *a*(Å) values from a, b and c samples (Table 1), we can observe that the increase in the quantity of manganese magnify the lattice parameters, which can be noted for a and c samples. The Mn^{+2} cation has a high diffusion in the octahedral interstices of the structures.

In Table 1, from Rietveld analysis it was obtained Sig ≤ 1.413 and $R_w \leq 21.228\%$. The Sig and R_w parameters show numerical coherence between calculated model and structure of phases. Moreover, the size of micrometrical crystallites is the same as that in literature [7,8].

The scanning electron microscopy shows particles average size smaller than 1 μm at 1100 °C calcination temperature (See Fig. 2). From Rietveld analysis of XRD showed crystallite average size between 0.576 and 0.626 μm which indicates agreement between both techniques. The magnetic property of phases and the van der Waals interactions contribute for the formation of particles clusters [18]. The smaller homogeneity of morphology implies in the presence of high concentrations of defects, which might influence the formation of ferromagnetic domains near the crystal surface. One may observe high chemical homogeneity in the SEM analysis of sample b.

The calculation of theoretical magnetization, in terms of Bohr magneton, used the distribution of cations in the spinel lattice obtained from Rietveld technique (Eqs. 3,4,5). This distribution is given by the formulae of a, b and c compositions at 1100 °C: a: (Ni Mg Mn $Fe_{0.81}$)[Ni Mg Mn $Fe]_2O_4$; b: (Ni Mg Co Fe)[Ni Mg Co $Fe]_2O_4$; c: ($^{3.168}$Ni Mg Mn Co Fe)[Ni Mg MnCo $Fe]_2O_4$. The Néel model was used so that the calculated magnetization is from ground state ($T=0$ K). It is noted the occupation of metallic cations (Ni^{+2}, Mg^{+2}, Mn^{+2}, Co^{+2} and Fe^{+3}) simultaneously in tetrahedral (A) and octahedral (B) sites of both formed structures. Therefore, the XRD analysis, associated with the Rietveld refinement, confirmed the inverse spinel feature of these materials [12,13,19].

$$M_{T(a)} = 5(Fe_{oct.} - Fe_{tet.}) + 5(Mn_{tet.} - Mn_{oct.}) + 2(Ni_{oct.} - Ni_{tet.})$$
$$= 24.\ 96\ \mu_B/cell$$
$$= 3.\ 12\ \mu_B \quad (3)$$

$$M_{T(b)} = 5(Fe_{oct.} - Fe_{tet.}) + 3(Co_{oct.} - Co_{tet.}) + 2(Ni_{oct.} - Ni_{tet.}) = 24.42\ \mu_B/cell = 3.05\ \mu_B \quad (4)$$

$$M_{T(c)} = 5(Fe_{oct.} - Fe_{tet.}) + 5(Mn_{tet.} - Mn_{oct.}) + 3(Co_{oct.} - Co_{tet.}) + 2(Ni_{oct.} - Ni_{tet.}) = 35.58\ \mu_B/cell = 4.55\ \mu_B \quad (5)$$

In Fig. 3, we observe the dependence of the magnetization with the applied magnetic field by means of the hysteresis cycle. The hysteresis cycles present low coercivity and low loss of energy in the field inversion.

The low losses in the inversion of the applied field indicate a magnetic material soft being dissipated little energy to reverse the magnetic flux [12,13,19]. The parameters of saturation magnetization and coercive field are found in Fig. 3. In c ferrite calcined at 1100 °C/3 h occurred an abrupt increase of saturation magnetization to 53.20 Am^2/Kg, which emphasizes the importance of the chemical composition for the magnetic properties.

We can note from theoretical calculations the coherence of results regarding that occurs agreement between increase of experimental and theoretical magnetization. The effects such as the chemical homogeneity, the concentration of defects and the volume of ferromagnetic domains increase or decrease the magnetization [7,8,18].

The coercive field is inversely proportional to M_s [9,10]. The b ferrite has the highest value of coercive field (H_c $2{,}96 \times 10^{-2}$ T). The fact that b has a hysteresis area with larger coercivity changes the absorbing properties of the material.

The plots of Fig. 4 show the relation between the theoretical magnetization in terms of spin angular momentum and the saturation magnetization in the investigated systems. We observe the direct relation between the theoretical magnetization (M_T) and experimental magnetization (M_s). The effect of experimental magnetization was larger for the addition of Mn with Co, whose the quantity of dopants is 0.05Mn/0.05 Co.

Fig. 5 depicts the reflectivity versus frequency GHz) plot of a, b and c ferrites. The material with 0.1 Co (b composition) has a large band in its absorption curve from 9 to 10.5 GHz. Moreover, it has a 3.0 mm deep enlargement in the absorbing band even when there is a decay in absorption. The 5.0 mm deep RAMs are optimized in frequency regions away from the analyzed band, i.e., in regions lower than 8.2 GHz, having 10.98 dB attenuation in GHz frequency, which prevents the visualization of maximum absorption. The general analysis of reflectivity tests shows that the value of coercive field^{-2} T) from b ferrite was preponderant in the absorption results than the depth of composites.

In Table 2, we observe that addition of 0.1 of Co imparts maximum coercive field, which is certainly the cause for the enlargement of frequency range and the increase of absorption percentage.

The analysis of the plots of Fig. 6 emphasizes the contribution of cobalt for the coercivity and reflectivity properties. The higher concentration of this dopant in b ferrite results in higher coercive field value. On the other hand, there is an inverse behavior for manganese dopant.

By comparing the plots of Fig. 6, we observe that there is a relation between coercivity and absorbing performance of the material where the maximum Co concentration corresponds to maximum absorption percentage (%*A*). We can note that the coexistence of manganese and cobalt decreases the absorption effect. According to literature, cobalt has strong magnetic anisotropy field [13,19]. In these materials this is associated with the increase of coercive field, H_c, and since the measure of anisotropic field of a material is extremely complex, we chose to measure H_c.

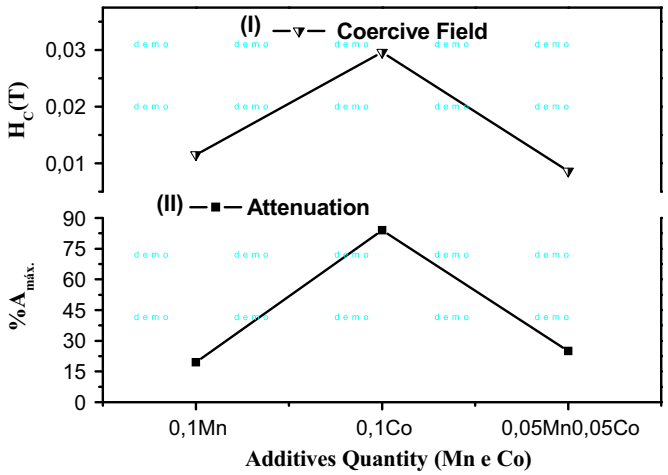

Fig. 6. Coercive field versus dopants quantity (I) and attenuation of microwave versus dopants quantity (II) of $NiMg_{0.1}M_xFe_2O_4$ composition, for *x*, a: 0.1 of Mn; b: 0.1 of Co and c: 0.05 Mn and 0.05 Co . Powder calcined at 1100 °C/3 h.

4. Conclusions

The manganese contributes for the increase of saturation magnetization in the structure keeping low coercive fields.

The cobalt improves the chemical homogeneity of b ferrite. The presence of these ions increases anisotropy of the material which means higher coercive field. In b ferrite, the absorption reached for specific values of analyzed frequencies. The result indicates that there is a strong influence of the coercive field in the effect of radiation absorption. We noted that the absorption effect is dependent upon the depth of the composite, the composition of the ferrimagnetic material and the frequency. The cobalt has magnetocrystaline anisotropy that causes the optimization of the results of reflectivity of spinel ferrite.

References

[1] R.C. Lima, J.C.S. Leandro, T. Ogasawara, Síntese e caracterização da hexaferrita de bário tipo m dopada com lantânio e sódio para utilização como absorvedor de microondas, Rev. Cerâm 49 (2003) 44–47.
[2] T.H. Ting, R.P. Yu, Y.N. Jau, Synthesis and microwave absorption characteristics of polyaniline/NiZn ferrite composites in 2 - 40 GHz, Mater. Chem. Phys. 126 (2011) 363–368.
[3] J.C. Dias, F.S. Silva, M.C. Rezende, Absorvedores de radiação eletromagnética aplicados no setor aeronáutico, Rev. Ciênc. Tecnol. 15 (2000) 33–42.
[4] L.C. Folgueras, M.C. Rezende, Processamento de material absorvedor de radiação eletromagnética a partir da impregnação de tecido de fibra de vidro com polímero condutor polianilina, Rev. Ciênc. Exatas 12 (2006) 155–160.
[5] I.C. Nlebedim, A.J. Moses, D.C. Jiles, Non-stoichiometric cobalto ferrite, $Co_xFe_{3-x}O4$ (*x*=1.0 to 2.0): Structural, magnetic and magnetoelastic properties, J. Magn. Magn. Mater. 343 (2013) 49–54.
[6] A.M. Gama, M.C. Rezende, C.C. Dantas, Dependence of microwave absorption properties on ferrite volume fraction in MnZn ferrite/rubber radar absorbing materials, J. Magn. Magn. Mater. 323 (2011) 2782–2785.
[7] U.R. Lima, M.C. Nasar, R.S. Nasar, J.H. Araújo, M.C. Rezende, Ni–Zn nanoferrite for radar-absorbing material, J. Magn. Magn. Mater. 320 (2008) 1666–1670.
[8] U.R. Lima, M.C. Nasar, R.S. Nasar, J.H. Araújo, M.C. Rezende, J.F. Oliveira, Synthesis of NiCuZn ferrite nanoparticles and microwave absorption characterization, Mater. Sci. Eng 151 (2008) 238–242.
[9] S. Verma, J. Chand, M. Singh, Effect of In^{+3} ions doping on the structural and magnetic properties of $Mg_{0,2}Mn_{0,5}Ni_{0,3}In_xFe_{2-x}O4$ spinel ferrites, J. Magn. Magn. Mater. 324 (2012) 3252–3260.
[10] S. Verma, A. Thakur, M. Singh, Study of non-magnetic Al^{+3} substituted mixed Mg-Mn-Ni ferrites for high frequency applications, Solid State Phys 1349 (2011) 1151–1152.
[11] L.J. Berchmans, R.K. Selvan, P.N.S. Kumar, C.O. Kumar, Augustin, Structural and electrical properties of $Ni^{1-x}Mg^xFe^2O^4$ systhesized by citrate gel process, J. Magn. Magn. Mater. 279 (1) (2004) 103–110.
[12] S.M. Patange, S.E. Shirsath, S.S. Jadhav, K.S. Lohar, D.R. Mane, K.M. Jadhav, Rietveld refinement and switching properties of Cr_{3+} substituted $NiFe^2O^4$ ferrites, Mater. Lett. 64 (2010) 722–724.

[13] C. Kittel, Física do Estado Sólido, 8th ed., Livros técnicos e científicos editora AS, In Rio de Janeiro (2006), p. 275–300.
[14] Y. Köseoglu, M.I.O. Oleiwi, R. Yilgin, A.N. Kocbay, Effect of chromium addition on the structural, morphological and magnetic properties of nano-crystalline cobalt ferrite system, Ceram. Int. 38 (2012) 6671–6676.
[15] L. Néel, Propriértés magnéticas des ferrites. Ferrimagnétisme et anti-ferromagnetisme, Ann. Phys 3 (1948) 137.
[16] D. Gherca, A. Pui, N. Cornei, A. Cojocariu, V. Nica, O. Caltun, Synthesis, characterization and magnetic properties of MFe^2O^4 (M= Co, Mg, Mn, Ni) nanoparticles using ricim oil as capping agent, J. Magn. Magn. Mater. 324 (2012) 3906–3911.
[17] S.K. Pradhan, S. Bid, M. Gateshki, V. Petkov, Microstructure characterization and cation distribution of nanocrystalline magnesium ferrite prepared by ball milling, Mater. Chem. Phys. 93 (2005) 224–230.
[18] R.C. Pessoa, M.C. Nasar, R.S. Nasar, M.C. Rezende, M.K. Hwang, Atennuation of incident radiation in composite of NiZn ferrite doped with magnesium and copper in epoxy, Rev. Cerâm 349 (2013) 59–64.
[19] D. Gherca, A. Pui, V. Nica, O. Caltun, N. Cornei, Eco-environmental synthesis and characterization of nanophase powders of Co, Mg, Mn and Ni ferrites, Ceram. Int. 40 (2014) 9599–9607.